Biologically Derived Soft Conducting Hydrogels Using Heparin-Doped Polymer Networks

Hangjun Ding,[†,‡] Mingjiang Zhong,[‡,#] Young Jo Kim,[§] Pitirat Pholpabu,[∥] Aditya Balasubramanian,[§] Chin Ming Hui,[‡] Hongkun He,[‡] Huai Yang,[⊥] Krzysztof Matyjaszewski,[‡,*] and Christopher John Bettinger[§,∥,*]

[†]School of Materials Science and Engineering, University of Science & Technology Beijing, 30 Xueyuan Road, Beijing 100083, People's Republic of China, [‡]Department of Chemistry, Carnegie Mellon University, 5000 Forbes Avenue, Pittsburgh, Pennsylvania 15213, United States, [§]Department of Materials Science and Engineering, Carnegie Mellon University, 5000 Forbes Avenue, Pittsburgh, Pennsylvania 15213, United States, [∥]Department of Biomedical Engineering, Carnegie Mellon University, 5000 Forbes Avenue, Pittsburgh, Pennsylvania 15213, United States, and [⊥]School of Engineering, Peking University, Beijing 100187, People's Republic of China. [#]Present address: Department of Chemistry and Department of Chemical Engineering, Massachusetts Institute of Technology, 77 Massachusetts Avenue, Cambridge MA 02215.

ABSTRACT The emergence of flexible and stretchable electronic components expands the range of applications of electronic devices. Flexible devices are ideally suited for electronic biointerfaces because of mechanically permissive structures that conform to curvilinear structures found in native tissue. Most electronic materials used in these applications exhibit elastic moduli on the order of 0.1−1 MPa. However, many electronically excitable tissues exhibit elasticities in the range of 1−10 kPa, several orders of magnitude smaller than existing components used in flexible devices. This work describes the use of biologically derived heparins as scaffold materials for fabricating networks with hybrid electronic/ionic conductivity and ultracompliant mechanical properties. Photo-cross-linkable heparin−methacrylate hydrogels serve as templates to control the microstructure and doping of *in situ* polymerized polyaniline structures. Macroscopic heparin-doped polyaniline hydrogel dual networks exhibit impedances as low as $Z = 4.17\ \Omega$ at 1 kHz and storage moduli of $G' = 900 \pm 100$ Pa. The conductivity of heparin/polyaniline networks depends on the oxidation state and microstructure of secondary polyaniline networks. Furthermore, heparin/polyaniline networks support the attachment, proliferation, and differentiation of murine myoblasts without any surface treatments. Taken together, these results suggest that heparin/polyaniline hydrogel networks exhibit suitable physical properties as an electronically active biointerface material that can match the mechanical properties of soft tissues composed of excitable cells.

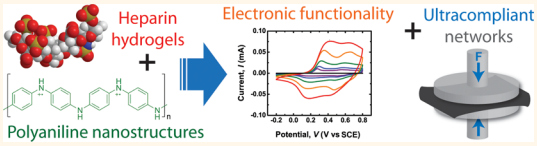

KEYWORDS: hydrogel · polymer · biomaterial · electronically active

Flexible electronics that utilize bendable and foldable components have potentially broad impact in many applications including clean energy, consumer electronics, and biomedical devices.[1,2] Conferring mechanical compliance and stretch-ability upon electronic devices permits conformability to curvilinear geometries and stable operation under strain.[3−5] Stretchable and flexible devices are ideally suited for the fabrication of electronic biointerfaces, systems that seamlessly meld viable tissue with external hardware.[6] Recent applications of flexible bioelectronic interfaces include conformal sensors for recording neuronal activity *in vivo*, large format multielectrode arrays for *in vivo* tissue stimulation, and sensor arrays for real time *in situ* monitoring of neuron electrophysiology during mechanical insults.[7,8] The intrinsic Young's modulus of many materials and devices used in these applications ranges from 0.1 to 1 MPa, values that preserve device functionality under physiologically relevant strains.[9,10] However, many electronically excitable cells and tissues in the human body including neurons and cardiac tissue exhibit Young's moduli between 1 and 10 kPa.[11] A mechanical mismatch at the biotic-abiotic interface can reduce the fidelity of electronic signal transduction through proposed mechanisms such as micromotion and loss of organotypic function.[12−16]

The ideal synthetic soft tissue biointerface would preserve electronic functionality while matching the mechanical properties of the native extracellular matrix of interest. Reducing the Young's modulus of electrically conductive structures from the megapascal (MPa) to the kilopascal (kPa)

* Address correspondence to km3b@andrew.cmu.edu, cbetting@andrew.cmu.edu.

Received for review November 21, 2013 and accepted April 16, 2014.

Published online April 16, 2014
10.1021/nn406019m

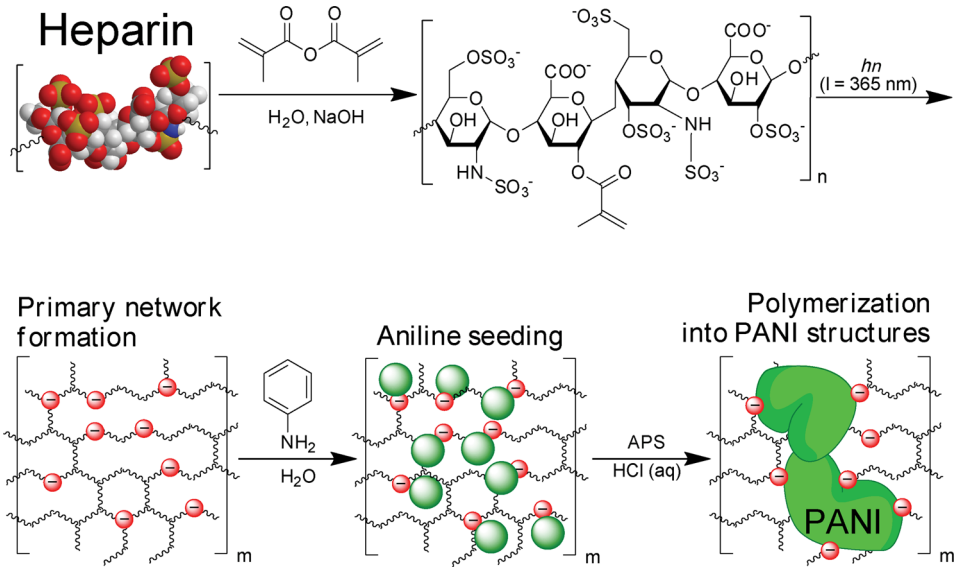

Scheme 1. Synthetic scheme of Hep-MA/PANI hydrogel dual networks. Photo-cross-linkable heparin was prepared *via* conjugation with methacrylate groups. Primary heparin gel networks were formed through photo-cross-linking of heparin-methacrylate (Hep-MA) at UV wavelengths (λ = 365 nm). Hep-MA gels were then loaded with ANI monomers, which were then converted into PANI structures *via in situ* oxidative polymerization.

regime requires coordinated synthesis and material processing strategies. Hydrogel-based biomaterials have been widely adopted as soft matter biointerfaces including applications in nonfouling coatings for biosensors and electronic tissue-device interfaces. Hydrogel-based electrodes are ideal for such applications because of the chemical diversity and swelling to reduce the polymer volume fraction in the hydrated elastic networks.[17] These properties can produce hydrogels with hybrid electronic/ionic conductivity and mechanical properties that are similar to native extracellular matrix proteins.[18]

Electronically active hydrogels have been prepared using several strategies including gelation of single-component precursors,[19] micropatterning of conducting polymers,[20] and *in situ* polymerization of aromatic monomers. These processing strategies can form interpenetrating networks of hydrogels with electronically active materials such as graphene,[21] poly(3,4 ethylenedioxythiophene) (PEDOT), polypyrrole (PPy), polyaniline (PANI), and other conjugated polymers.[22−30] Small molecules can also be used for simultaneous doping and cross-linking of conjugated precursors.[31] Here, we describe the design, synthesis, and fabrication of dual networks composed of photo-cross-linkable heparin−methacrylate hydrogels and PANI nanofibers formed by *in situ* oxidative polymerization. These composite materials exhibit ultracompliant mechanical properties, maintain exceptional electrical conductivity, and support the adhesion and differentiation of myoblasts *in vitro*.

RESULTS AND DISCUSSION

Synthesis, Preparation, and Characterization of Primary Heparin Networks. Swollen hydrogels represent an ideal class of starting materials for the synthesis and fabrication of ultracompliant electronically active biomaterials. Heparin was chosen as the primary hydrogel network because it is a naturally occurring biopolymer that can be functionalized in mild conditions. Heparins exhibit high anionic charge densities to promote large swelling ratios in water. Pendant sulfonate groups serve as strongly acidic groups to dope PANI. The degree of doping in PANI governs the intrinsic conductivity of secondary conjugated polymer network.[32] Heparin−methacrylate (Hep-MA) was selected as the primary network precursor, which can be cross-linked into networks *via* photoinduced free radical polymerization (Scheme 1). Equilibrium swelling ratios in water of $Q > 10$ suggest that anionic Hep-MA hydrogels are ideally suited for *in situ* polymerization of aniline (ANI) to form electrically active hydrogels composed of Hep-MA/PANI dual networks.

Heparins reacted with methacrylic anhydride (MA) yield Hep-MA through esterification. The final degree of substitution (DS) from this procedure ranges 40 $\pm$ 5% on a per tetramer (4-unit repeat) basis. The kinetics of the network formation was studied by measuring methacrylate consumption by ^{1}H nuclear magnetic resonance (NMR) spectroscopy. Methacrylate conversion was linear with time. The reaction rate was directly proportional to the heparin concentration (Figure 1). These data suggest that the polymerization rate follows zero-order reaction kinetics under these conditions. Hep-MA network formation requires initial precursor concentrations (hereby referred to as $[\text{Hep-MA}]_0$) larger than 2% (w/w). Gelation times ranged from 60 min for Hep-MA_{02} (Hep-MA precursor concentrations of 2% w/w) to 25 min for Hep-MA_{08}

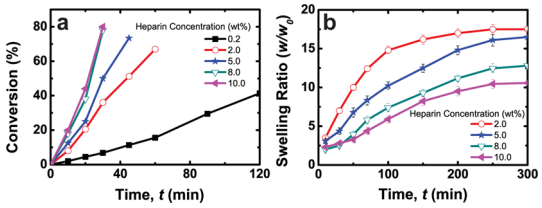

Figure 1. Photo-cross-linkable primary heparin networks showed large equilibrium swelling ratios. (a) The kinetics of methacrylate conversion in Hep-MA networks as a function of $[Hep\text{-}MA]_0$. Primary network formation requires aqueous precursor solutions of [Hep-MA] >2% (w/w). (b) The swelling kinetics of primary Hep-MA networks. Equilibrium swelling ratios were achieved after 4 h of swelling and exhibit $Q > 10$ for networks for all values of $[Hep\text{-}MA]_0$ in this study.

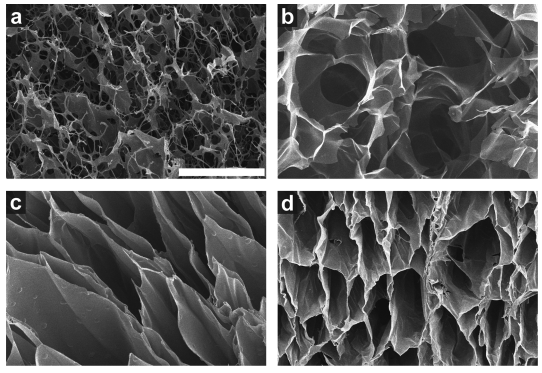

Figure 2. Primary Hep-MA networks are microporous. SEM images indicate the formation microporous networks with strut thicknesses that correlate with Hep-MA concentration. Networks were prepared from precursor solutions with the following concentrations of $[Hep\text{-}MA]_0$ (a) 2, (b) 5, (c)8, and (d) 10% (w/w). The scale bars represent 50 μm, and all images were recorded at identical magnification.

and $Hep\text{-}MA_{10}$ (precursor concentrations of 8% and 10% w/w, respectively) (Figure 1). Equilibrium swelling ratios of primary Hep-MA networks ranged from 10.5 ± 0.8 to 17.5 ± 2.5 for $Hep\text{-}MA_{10}$ and $Hep\text{-}MA_{02}$, respectively (Figure 1, Table S1). Hep-MA networks are composed of interconnected porous networks with wall thicknesses that positively correlate with $[Hep\text{-}MA]_0$. $Hep\text{-}MA_{02}$ networks exhibit partially formed pores (Figure 2) with poor mechanical integrity. Hep-MA networks prepared using precursor solutions of $[Hep\text{-}MA]_0 \geq 5\%$ (w/w) exhibit a robust disordered cellular structure with pore diameters of approximately 30 μm (Figure 2c,d). The compressive Young's moduli of swollen Hep-MA networks ranges from 8.0 ± 1.5 to 100 ± 9.8 kPa for $Hep\text{-}MA_{02}$ and $Hep\text{-}MA_{10}$ gels, respectively (Figure 3). These data confirm a positive correlation between $[Hep\text{-}MA]_0$ and Young's modulus. $Hep\text{-}MA_{02}$ networks exhibit viscoelastic behavior that is characterized by storage moduli G' values in the sub-kPa regime that exhibit a marginal frequency dependence. Hep-MA networks prepared from $[Hep\text{-}MA]_0$ >5% (w/w) exhibit frequency-independent values for G' which are significantly larger that corresponding values for G'' (Figures 3 and S1). These data indicate that swollen Hep-MA hydrogels are compliant yet elastic, making them ideal networks for *in situ* PANI polymerization. $Hep\text{-}MA_{05}$ was selected as the primary network composition for PANI incorporation because it exhibits the smallest storage modulus while maintaining well-defined interconnected macropores.

***In Situ* Formation of Polyaniline Networks.** PANI is a well-characterized conducting polymer that can be synthesized within hydrogel networks *via in situ* oxidative polymerization.[30,33] PANI was incorporated into Hep-MA hydrogels through *in situ* polymerization and served as the electronically conducting component in dual networks (Scheme 1). Pendant sulfonic acid groups in Hep-MA were concurrently regenerated *via* ion-exchange of sodium sulfonate of the heparin salt during *in situ* polymerization. The macroscopic properties of the gel were preserved during this processing step.

The incorporation of secondary PANI networks into primary Hep-MA hydrogels was verified *via* FT-IR spectroscopy (Figure 4c). All of the prominent signatures of acid-doped PANI emeraldine salts are present: C═C stretching deformation of quinoids and benzenoid rings at 1580 and 1496 cm^{-1}; C—N stretching of secondary aromatic amines at 1302 cm^{-1} and in-plane bending of C—H in aromatic moieties at 1141 cm^{-1}.[34] The absorption peak at 1600 cm^{-1} was assigned to the carbonyl groups in heparin, which indicated integration of primary Hep-MA networks with PANI. UV—vis spectra (Figure 4d) exhibited prominent features at λ = 440 and λ > 800 nm. These peaks indicated the presence of doped PANI networks within primary Hep-MA gels.[35] Taken together, these results suggest that strongly acidic pendant sulfonic acid groups within Hep-MA hydrogels can dope secondary PANI networks.

The electrical properties of PANI networks were governed by controlling the ratio of initial concentrations of aniline ($[ANI]_0$) and ammonium persulfate, APS, ($[APS]_0$) during *in situ* PANI polymerization. The oxidation state and therefore the electrical properties of PANI can be influenced by the polymerization conditions.[36] Here, *in situ* oxidative polymerization of ANI preloaded within Hep-MA gels at $[ANI]_0$:$[APS]_0$ = 8:1 produced a dark green coloration, confirming the presence of highly conductive emeraldine salts within the Hep-MA/PANI dual network. UV—vis spectra of Hep-MA/PANI gels suggested that the PANI was partially oxidized (Figure S2). Preloading of ANI monomers into Hep-MA hydrogels presented additional challenges in controlling the physical properties of the dual network. The ratio of $[ANI]_0$:$[APS]_0$ = 8:1 used for *in situ* PANI polymerization in this study was larger than the typical ratio of $[ANI]_0$:$[APS]_0$ = 1:1 that was usually used for ANI polymerization in solution.[37] A higher relative concentration of ANI was used in this study because the initial polymerization reactions occurred

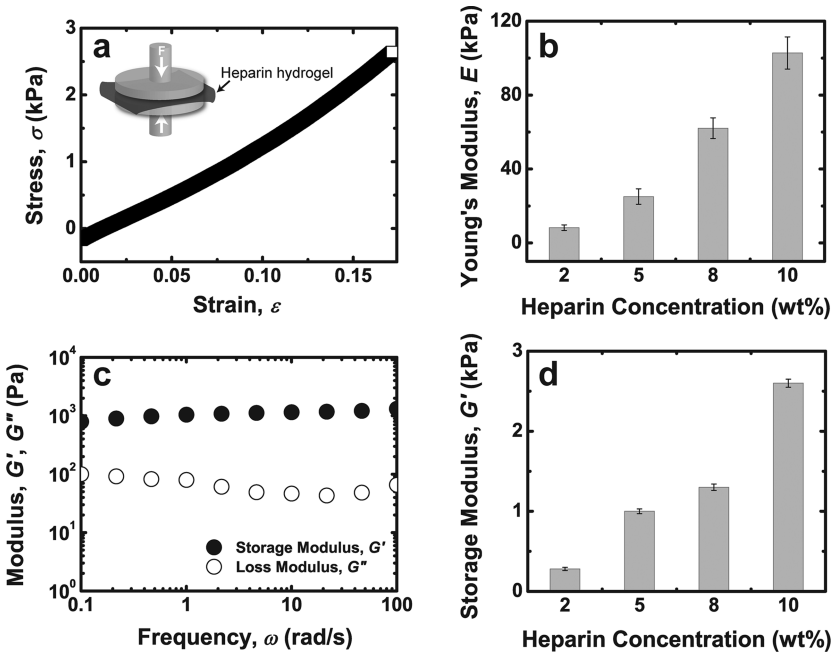

Figure 3. Mechanically compliant photo-cross-linked Hep-MA primary hydrogel networks. (a) Representative stress−strain plots of Hep-MA$_{05}$ hydrogels under compression shown along with (b) extracted values for Young's modulus. (c) Frequency sweeps of Hep-MA$_{05}$ networks indicated that the storage and loss moduli of gels varied only slightly for ω between 0.1 and 100 rad s^{-1}. (d) A summary of the values for storage modulus G' at ω = 100 rad s^{-1} is shown for heparin-based networks as a function of [Hep-MA]$_0$.

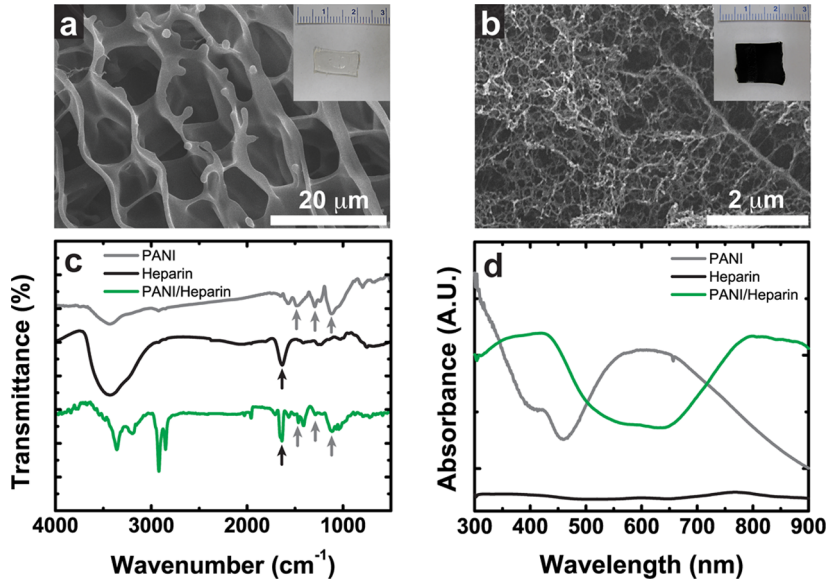

Figure 4. Hep-MA/PANI dual networks formed *via in situ* PANI polymerization. SEM micrographs of Hep-MA primary networks (a) before and (b) after PANI polymerization indicated the formation of secondary PANI networks within the microporous structures of Hep-MA. Insets show macroscopic photographs. The formation of dual networks was confirmed through (c) FT-IR, and (d) the UV−vis absorption spectra of the PANI networks indicate that these networks are composed of partially reduced emeraldine salt (ES).

primarily at the macroscopic interface of the ANI-loaded Hep-MA gels. The surrounding solution can serve as a reservoir of APS that can then diffuse into the gel and react. Hep-MA/PANI networks prepared using [ANI]$_0$:[APS]$_0$ = 1:1 during *in situ* polymerization produces overoxidized PANI as inferred by the absence of emeraldine salts. The consequent formation of pernigraniline, the insulating form of PANI, was inferred from the dark violet coloration after PANI polymerization. In the case when [ANI]$_0$:[APS]$_0$ = 16:1, APS was rapidly depleted prior to the formation of percolating PANI networks. This was inferred from the formation of brown PANI oligomer within cross-linked Hep-MA gels. The absolute concentration of ANI was

also critical during *in situ* oxidative polymerization of secondary PANI networks. The rate of PANI polymerization increased with $[APS]_0$ and $[ANI]_0$ increase.[38] Rapid PANI polymerization precluded the diffusion of ANI monomer throughout the primary Hep-MA network forming an impenetrable PANI film at the gel interface (Figure 7d). Nascent PANI structures formed on the surface occluded pores within the primary Hep-MA network, rendering the remaining volume inaccessible and ultimately preventing the formation of uniform percolating PANI networks.

Hep-MA_{05}/PANI dual networks were composed of a percolating network of PANI nanofibers (approximate diameter of 50 nm) within a macroporous heparin network (Figure 4). PANI networks were integrated within the Hep-MA as no PANI precipitate was dislodged from the dual networks. These data suggested that macroporous Hep-MA networks serve both as a template for electrostatic stabilization and *in situ* formation of percolating PANI nanostructures. This observation is in agreement with previous reports that described the spontaneous and selective formation of PANI nanofibers in the presence of organic templates.[38] These results corroborate previous work in which the geometry of PANI nanostructures can be controlled by polymerization conditions.[39] The precise mechanism for controlling PANI morphology has yet to be elucidated.[40] Amphiphilic ANI monomers are implicated in the spontaneous formation of energetically stable micelles.[41] The interconnected porous structure of primary Hep-MA networks promotes the formation of high aspect ratio PANI structures, which can ultimately form percolating structures. The high anionic density of Hep-MA networks increased the loading of protonated ANI monomers into the gels through direct Columbic interactions. These advantageous properties of heparin gels have been utilized in the template fabrication of other conducting polymer structures.[42]

Mechanical and Electrical Characterization of Dual Heparin/Polyaniline Networks. Incorporating percolating PANI nanostructures increased the storage modulus from 800 ± 80 to 900 ± 100 Pa (Figure 5a). These data suggested that the mechanical properties of the primary Hep-MA hydrogel networks were largely preserved, despite the addition of secondary PANI networks. The impact of PANI structures on the bulk Hep-MA_{05} hydrogel mechanical properties can be attributed to several physical properties. The porous microstructure of Hep-MA_{05} produced PANI nanofibers that create conductive percolating networks despite low volume fractions. Strongly anionic pendant sulfonate domains in the heparin backbone promoted a high swelling ratio Q in aqueous environments. A value of $Q > 10$ ensures that the physical properties of the polymer network can be predicted by an extrapolation of the de Gennes model for semidilute solutions.[43] Finally, semiflexible rod-like PANI molecules exhibited

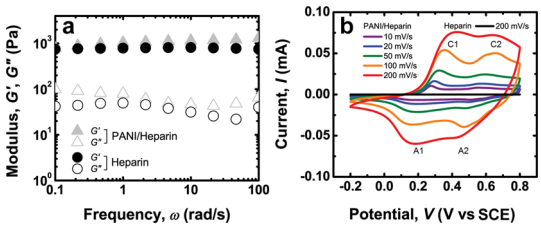

Figure 5. Incorporating secondary PANI networks generated redox activity without significantly impacting mechanical properties. (a) Frequency sweeps of Hep-MA_{05} and Hep-MA_{05}/PANI gels indicate an increase in storage modulus of approximately 12% upon addition of the secondary PANI networks. (b) Cyclic voltammetry sweeps (second cycle) of networks composed of pristine Hep-MA_{05} and Hep-MA_{05}/PANI hydrogel networks. Two oxidation (cathodic) peaks (C_1/C_2) and two reduction (anodic) peaks (A_1/A_2) correspond to redox activity of integrated PANI networks that transition between leucoemeraldine, emeraldine, and pernigraniline compositions (see text). Redox activity was stable over repeated cycling (see Supporting Information).

intrinsic mechanical flexibility by virtue of freely rotating bonds on the polymer backbone.

Cyclic voltammograms suggested that PANI structures within Hep-MA_{05}/PANI dual networks were pseudocapacitive with two sets of redox peaks (C_1/A_1, C_2/A_2) (Figure 5b). The first redox peak (C_1/A_1) defines the transition between semiconducting leucoemeraldine and electronically conducting polaronic emeraldine form. The Faradaic transformation of emeraldine to the fully oxidized pernigraniline was indicated by an additional redox peak (C_2/A_2).[44] Redox activity was largely absent from the primary pristine Hep-MA networks, which indicated that the secondary PANI networks were responsible for the observed features in the cyclic voltammograms. Peak anodic and cathodic currents increase with increasing scan rate. Oxidation (C_1/C_2) and reduction (A_1/A_2) peaks are shifted to more positive and negative potentials, respectively, as the scan rate is increased. These data indicate that redox reactions in PANI structures are quasi-reversible.

Hybrid electronic/ionic conductivity of Hep-MA_{05}/PANI networks was strongly dependent on $[ANI]_0$ during *in situ* polymerization. Hep-MA_{05}/PANI networks formed using $[ANI]_0 = 0.1$ and 0.5 M exhibited impedances of approximately 2×10^4 and 1×10^4 Ω at 0.01 Hz. Low-frequency impedances were significantly higher than those in Hep-MA_{05}/PANI networks formed using $[ANI]_0 = 1$ M, which exhibited an impedance of approximately 900 Ω at 0.01 Hz (Figure 6). The low frequency impedance was smaller than many previously reported values for conducting hydrogels.[15,45,46] These data can be attributed to the high surface area of the macroporous Hep-MA networks and nanostructured PANI in swollen Hep-MA/PANI dual networks. Incorporating secondary PANI networks using any value of $[ANI]_0$ reduced the impedance at 1 kHz of pristine Hep-MA_{05} networks from $Z = 34$ Ω to a range of $Z = 4.17-6.06$ Ω.

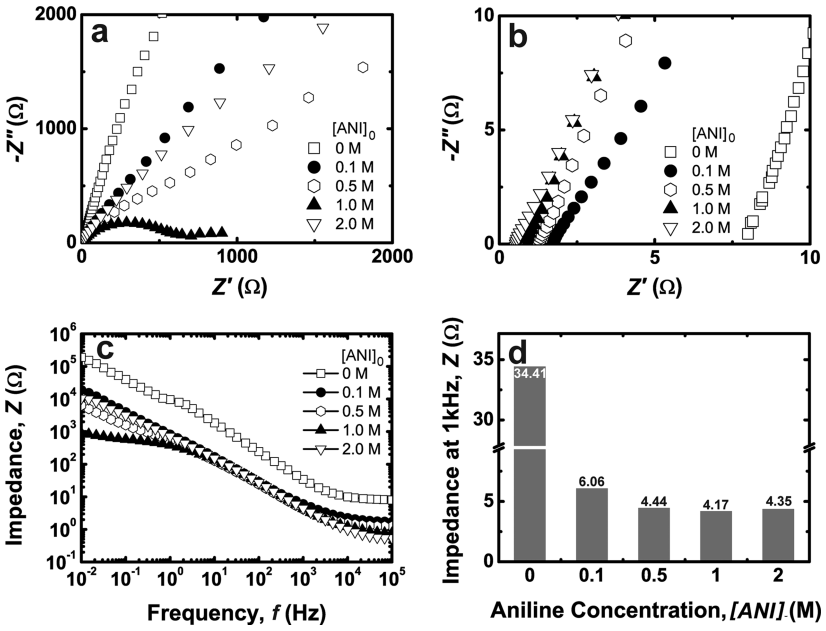

Figure 6. Characterization of Hep-MA$_{05}$/PANI networks using electrochemical impedance spectroscopy. (a) The full spectrum and (b) high frequency regime of Nyquist plots shown for Hep-MA$_{05}$/PANI networks as a function of [ANI]$_0$. (c) Bode plots of Hep-MA$_{05}$/PANI networks shown for frequencies *f* between 0.01 Hz and 100 kHz. (d) Impedance values at *f* = 1 kHz shown for Hep-MA$_{05}$/PANI networks prepared using a variety of values for [ANI]$_0$.

Hep-MA$_{05}$/PANI networks formed using [ANI]$_0$ = 1 M exhibited a projected low-frequency real term impedance *Z*′(Re) of 600 Ω.[47] Nyquist plots of Hep-MA$_{05}$/PANI networks prepared using [ANI]$_0 \neq$ 1 M suggested that the impedance was dominated by a constant phase element (CPE) that can be represented by $Z_{CPE} = 1/[A(j\omega)^{\alpha}]$ where *A* and α are constants, the latter of which is related to the phase angle in the Nyquist plot.[48] The CPE exhibits Warburg-like behavior where $\alpha \neq 0.5$ and was a strong function of [ANI]$_0$ employed during polymerization. The presence of CPE suggests that these hydrogels exhibit a nonideal capacitance originating from inhomogeneous conductivity, microstructural defects in PANI,[49] or electrode materials with blocked diffusion.[50] The complex microstructure and large thicknesses (~1 mm) precluded the application of established models to measure the relative contributions of electronic conduction (*via* PANI) and ionic conduction (*via* swollen Hep-MA).[51,52] Practical applications of these materials as bioelectronic interfaces require thicknesses significantly larger than 100 μm to prevent cells on the apical surface to sense the stiffness of the underlying substrate.[53]

Hep-MA$_{05}$/PANI networks prepared using [ANI]$_0$ = 1 M exhibited a robust green coloration (Figure 4b; Figure S2) and an absorption spectrum (Figure 4d) that is consistent with electrically conducting emeraldine salt.[35] These data suggest that pendant sulfonates in Hep-MA have sufficient density and strength to dope PANI networks. The [ANI]$_0$-dependent behavior in *Z* can be explained by PANI morphology within Hep-MA$_{05}$/PANI networks (Figure 7; Figure S3). *In situ* polymerization of ANI produced networks in the subpercolation threshold for [ANI]$_0$ < 1 M. Conversely, Hep-MA$_{05}$/PANI networks formed using [ANI]$_0$ > 1 M produced solid PANI films that occluded the macroporous network and reduced network conductivity by eliminating PANI percolation and long-range ion diffusion. Hep-MA$_{05}$/PANI networks formed using [ANI]$_0$ > 1 M produced PANI structures with a dark blue coloration. These data suggest that the PANI networks are composed of partially doped emeraldine base (EB) due to insufficient sulfonate groups of Hep-MA. Highly conductive Hep-MA$_{05}$/PANI networks synthesized using [ANI]$_0$ = 1 M were the only compositions studied in this work that exhibited a percolating nanofiber PANI morphology (Figure 7c), which has been previously associated with highly conducting hydrogel networks.[25] The impedance of Hep-MA$_{05}$/PANI networks may be further reduced by controlling PANI morphology. Altering [ANI]$_0$ impacts the self-assembly of PANI structures during polymerization.[54−56] Poly(2-acrylamido-2-methylpropanesulfonic acid) (PAMPSA) can dope and template PANI into nanometer-scale electrically conductive nanostructures.[57−59] Yoo *et al.* showed that the molecular weight of strongly acidic PAMPSA templates can influence PANI conductivity.[60] Parallel methodologies may be used to control the morphology and conductivity of PANI structures in Hep-MA networks.

***In Vitro* Biocompatibility of Heparin−Polyaniline Dual Hydrogel Networks.** Hep-MA/PANI networks supported C2C12 murine myoblast adhesion and differentiation. Untreated pristine networks promote rapid adhesion

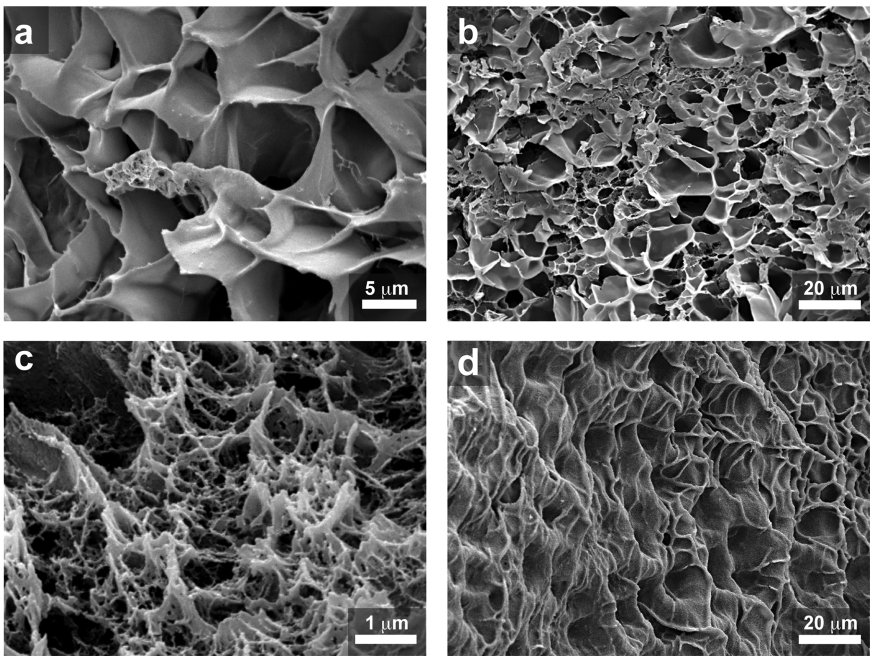

Figure 7. The morphology of secondary PANI networks formed from *in situ* polymerization of ANI as a function of $[ANI]_0$. SEM images of Hep-MA_{05}/PANI dual networks shown for the following values of $[ANI]_0$ used during precursor loading: (a) 0.1, (b) 0.5, (c) 1.0, and (d) 2.0 M, respectively. The ratio of $[APS]_0$ to $[ANI]_0$ was kept constant at 1:8 for all Hep-MA_{05}/PANI networks. $[ANI]_0$ = 0.1 M produce (a) PANI oligomers in the subpercolation threshold. Increasing $[ANI]_0$ produced continuous PANI networks, evident by percolating PANI structures in (b−d).

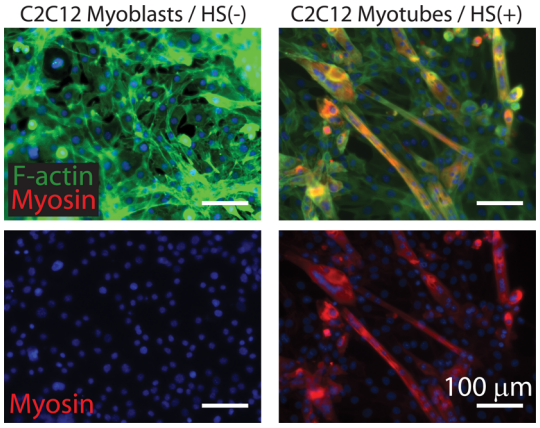

Figure 8. Hep-MA_{05}/PANI dual networks capable of promoting adhesion, proliferation, and differentiation of excitable cells. C2C12 myoblasts adhered to Hep-MA_{05}/PANI substrates without the need for surface treatments and (a) proliferated into confluent monolayers after 3 weeks in proliferation medium (HS(−)). Fluorescent micrographs (Myosin, Rhodamine; F-actin, FITC; DAPI) of C2C12 myotubes after 5 days in differentiation medium (HS(+)) suggest that Hep-MA_{05}/PANI substrates were permissive of C2C12 differentiation.

and spreading of myoblasts within 24 h. This is likely due to the efficient physisorption of proteins on heparin-based networks.[61] Myoblasts proliferated to form a confluent layer within 3 days. Myoblasts were then differentiated into myotubes as indicated through the formation of elongated morphologies and the presence of myosin (Figure 8). Hep-MA_{05}/PANI networks promoted cell adhesion without exogenous ligands. C2C12 cells cultured on both Hep-MA_{08}/PANI and Hep-MA_{10}/PANI networks exhibited comparable morphology before and after myotube differentiation (Figures S7−S9). Myotubes differentiation was confirmed by the presence of myosin. Taken together, this class of heparin-based conducting hydrogels showed a promising cross-section of biocompatibility and physical properties for electrode materials as long-term *in vitro* tissue sensing and stimulation platforms.[12,62,63] Enzymatic degradation of primary heparin networks could also permit the fabrication of biodegradable conducting polymeric medical materials.[29,64,65]

CONCLUSIONS

Hep-MA/PANI networks offer a unique combination of mechanical compliance and hybrid electronic/ionic conductivity. The redox behavior and projected DC conductivity (based on Z'(Re) of 600 Ω at ω = 0.01 Hz) is comparable to previous reports of conducting hydrogels.[28] Furthermore, Hep-MA/PANI networks exhibit ultracompliant mechanical properties and permit myoblast adhesion and differentiation. These collective properties of biologically derived primary heparin gels suggest that Hep-MA/PANI networks have strong potential for many biomedical applications. For example, these materials could be engineered to match the mechanical modulus of excitable cells for use as materials to monitor the long-term electronic activity of tissues while maintaining organotypic function. Photolithography can be used to fabricate microstructures composed of UV photo-cross-linkable heparins while maintaining feature fidelity. Compliant biologically

derived conducting materials with improved environmental stability may be suitable for potential use as a material for ingestible electronics,[66,67] electroceuticals,[68] or energy storage.[31,69]

METHODS

Synthesis and Characterization of Heparin−Polyaniline Dual Networks. All materials were procured from Sigma-Aldrich (St. Louis, MO) and used as received unless otherwise stated. Aqueous solutions of heparin (0.2−10% w/w) were prepared using 5 M NaOH. Photo-cross-linkable heparin−methacrylate (Hep-MA) precursors were prepared by combining heparin (porcine source, $M_w \sim 17-19$ kDa) incubated with methacrylic anhydride (MA) and adjusted to pH = 8. The degree of substitution (DS) of methacrylate groups covalently linked to heparin precursors was measured by ^{1}H nuclear magnetic resonance (Bruker Avance 300 MHz, Billerica, MA). The DS was determined from integral ratios of peaks of the methacrylate groups at 6.2 ppm compared to peak corresponding to methyl groups in heparin at 2.05 ppm. Solutions used for photopolymerization were incubated with 2-methyl-1-[4-(hydeoxyethoxy)phenyl]-2-methyl-1-propanone (Irgacure 2959) to create final concentrations of 0.5% (w/w) of photoinitiator. Gels were photo-cross-linked using UV illumination for 30−60 min (λ_{max} = 365 nm, 10 mW/cm^2, Blak-Ray, Upland, CA). The swelling ratio Q of Hep-MA gels was determined by gravimetry *via* the following expression where W_0 and $W(t)$ are the mass of networks before and after hydration:

$$Q(t) = \frac{W(t) - W_0}{W_0} \quad (1)$$

Hep-MA/PANI dual-networks were formed by sequentially incubating cross-linked Hep-MA hydrogels in aqueous solutions of ANI ($[ANI]_0$, between 0.1 and 2 M, 10 min) and acidic solutions of APS ($[APS]_0$, between 12.5 mM and 2 M, 20−120 min). The gel fraction of Hep-MA/PANI dual networks was recovered by washing in ddH_2O (5×) after oxidative polymerization.

Mechanical and Morphological Characterization of Networks. Compression tests were conducted (Instron 5943 equipped with Bluehill 3 software, Norwood, MA) using a 10 N load cell. A strain rate of 1 mm min^{-1} was applied to the sample until failure. The Young's modulus was calculated using the stress−strain slope between ε = 0 and 5% (n = 5). The storage and loss moduli of Hep-MA-based hydrogel networks, both with and without secondary PANI networks, were measured using a rheometer (HR-2, TA Instruments, New Castle, DE) operating at room temperature. A strain amplitude of 0.5% was used to ensure that hydrogel networks remained in the linear viscoelastic regime during measurements (n = 4). Hep-MA networks dedicated for SEM imaging were lyophilized for 24 h, coated with 4 nm of Pt (Emtech K575X, Quorum Technologies, Guelph, ON, Canada) and imaged (Philips XL-30 FEG, FEI, Hillsboro, OR).

Chemical and Electrical Characterization of Hydrogel Networks. Samples dedicated for structural characterization using FT-IR (64 scans, Mattson ATI Affinity 60AR, Fremont, CA) were prepared by drop-casting dilute solutions of dichloromethane on KBr windows. UV−vis spectra (PerkinElmer Lambda 900, Waltham, MA) were recorded for Heparin-MA and Hep-MA/PANI dual networks. The electrical conductivity of Hep-MA and Hep-MA/PANI hydrogel networks was measured by electrochemical impedance spectroscopy (EIS) at frequencies from 0.01 Hz to 100 kHz and an AC perturbation of 5 mV (VMP3, BioLogic Science Instruments, Grenoble, France). The impedance of Hep-MA/PANI hydrogels was measured using two-terminal stainless electrodes using a custom cell fabricated from PTFE. A swollen Hep-MA/PANI film in 1 M HCl solution (nominal sample surface area = 0.5 × 0.5 cm^2) was inserted between two stainless current collectors to form a sandwich-like cell.[54] Hep-MA/PANI films synthesized at different $[ANI]_0$ with identical dimensions were characterized by EIS for systematic comparison. Cyclic voltammetry (CV) curves were performed in 1 M H_2SO_4 solution using potentials between −0.2 and 0.8 V *vs* saturated calomel electrode (SCE) reference electrode at a sweep rate of 10−200 mV s^{-1} for multiple cycles. All electrochemical measurements were carried out using a multichannel potentiostat (VMP3, Biologic, Knoxville, TN). A three-electrode system was equipped with a working electrode (Hep-MA/PANI gels on glassy carbon (GC) electrode), a platinum counter electrode, and a saturated calomel electrode (SCE) as the reference electrode. GC electrodes (diameter = 3 mm, Gamry, Warminster, PA) were polished with diamond paste (successive sizes of 3, 1, and 0.25 μm) and washed with ddH_2O and acetone before drying in air. Nafion 117 solution (5% w/w) was diluted 1:10 in ethanol (100%), coated onto GC electrodes, and allowed to air-dry. Hep-MA/PANI gels were dipped into the Nafion solution and then mechanically laminated to coated GC electrodes.

Cell Adhesion and Differentiation. Cell culture supplies were acquired from Invitrogen (Carlsbad, CA) unless otherwise stated. Hep-MA/PANI gels were sterilized in 70% (v/v) ethanol for 2 h, washed three times with 1× PBS, and placed in a 24-well plate. Substrates were equilibrated for 24 h in proliferation culture medium composed of Dulbecco's Modified Eagle Medium (DMEM) supplemented with 10% fetal bovine serum (FBS) and 1% penicillin/streptomycin (P/S). C2C12 myoblasts (ATCC, Monassas, VA) were seeded on Hep-MA/PANI gels (1 mL of 10^6 cells/mL suspension) and grown in culture medium for 3 weeks until the substrates were approximately 80% confluent. Polystyrene control substrates were cultured for 3 days. Myoblast differentiation was induced by incubating cells in DMEM with 2% horse serum (HS(+)) and 1% P/S for 5 additional days. Myoblasts and differentiated myotubes were fixed in 4% formaldehyde for 20 min and stained as follows: 1° antibody, myosin mouse monoclonal antibody (clone MY32, Life Science Technologies, Grand Island, NY); 2° antibody, goat anti-mouse Alexa Fluor 546 (Life Science Technologies). F-actin was stained using 20 μL of Alexa Fluor 488 Phalloidin (200 U/mL) and counterstained with SlowFade Gold Antifade Reagent with DAPI. Fluorescent images were recorded using an EvosFL microscope (Advanced Microscopy Group, Bothell, WA).

Conflict of Interest: The authors declare no competing financial interest.

Acknowledgment. Funding provided by the following organizations: the Shurl and Kay Curci Foundation, the Berkman Foundation, the American Chemical Society Petroleum Research Fund (ACS PRF #51980-DNI7), the National Science Foundation DMR 09-69301 and the National Institutes of Health (NIH; R21EB015165), U.S. Army Materiel Command (W81XWH1210626), the National Natural Science Foundation of China (NSFC51273022). NMR instrumentation at CMU was partially supported by National Science Foundation (CHE-0130903 and CHE-1039870). The authors also acknowledge the support from Molecular Biosensor & Imaging Center in Carnegie Mellon University.

Supporting Information Available: Physical data on heparin hydrogel networks; rheological characterization of heparin hydrogels; UV−vis spectra and photographs of secondary PANI networks with different doping levels; additional CV data; proposed model for structure−property relationships during secondary PANI network formation; additional fluorescent micrographs of C2C12 cells cultured on Hep-MA/PANI dual networks. This material is available free of charge *via* the Internet at http://pubs.acs.org.

REFERENCES AND NOTES

1. Someya, T.; Sekitani, T.; Iba, S.; Kato, Y.; Kawaguchi, H.; Sakurai, T. A Large-Area, Flexible Pressure Sensor Matrix with Organic Field-Effect Transistors for Artificial Skin Applications. *Proc. Natl. Acad. Sci. U.S.A.* **2004**, *101*, 9966–9970.

2. Sekitani, T.; Someya, T. Stretchable, Large-Area Organic Electronics. *Adv. Mater.* **2010**, *22*, 2228–2246.
3. Sekitani, T.; Noguchi, Y.; Hata, K.; Fukushima, T.; Aida, T.; Someya, T. A Rubberlike Stretchable Active Matrix Using Elastic Conductors. *Science* **2008**, *321*, 1468–1472.
4. Rogers, J. A.; Someya, T.; Huang, Y. Materials and Mechanics for Stretchable Electronics. *Science* **2010**, *327*, 1603–1607.
5. Vosgueritchian, M.; Lipomi, D. J.; Bao, Z. Highly Conductive and Transparent PEDOT:PSS Films with a Fluorosurfactant for Stretchable and Flexible Transparent Electrodes. *Adv. Funct. Mater.* **2012**, *22*, 421–428.
6. Viventi, J.; Kim, D.-H.; Moss, J. D.; Kim, Y.-S.; Blanco, J. A.; Annetta, N.; Hicks, A.; Xiao, J.; Huang, Y.; Callans, D. J.; *et al.* A Conformal, Bio-Interfaced Class of Silicon Electronics for Mapping Cardiac Electrophysiology. *Sci. Transl. Med.* **2010**, *2*, 24ra22.
7. Morrison, B., III; Elkin, B. S.; Dolle, J.-P.; Yarmush, M. L. *In Vitro* Models of Traumatic Brain Injury. *Annu. Rev. Biomed. Eng.* **2011**, *13*, 91–126.
8. Graudejus, O.; Morrison, B.; Goletiani, C.; Yu, Z.; Wagner, S. Encapsulating Elastically Stretchable Neural Interfaces: Yield, Resolution, and Recording/Stimulation of Neural Activity. *Adv. Funct. Mater.* **2012**, *22*, 640–651.
9. Lacour, S. P.; Wagner, S.; Huang, Z.; Suo, Z. Stretchable Gold Conductors on Elastomeric Substrates. *Appl. Phys. Lett.* **2003**, *82*, 2404–2406.
10. Li, T.; Huang, Z.; Suo, Z.; Lacour, S. P.; Wagner, S. Stretchability of Thin Metal Films on Elastomer Substrates. *Appl. Phys. Lett.* **2004**, *85*, 3435–3437.
11. Green, M. A.; Bilston, L. E.; Sinkus, R. *In Vivo* Brain Viscoelastic Properties Measured by Magnetic Resonance Elastography. *NMR Biomed.* **2008**, *21*, 755–764.
12. Bhana, B.; Iyer, R. K.; Chen, W. L. K.; Zhao, R.; Sider, K. L.; Likhitpanichkul, M.; Simmons, C. A.; Radisic, M. Influence of Substrate Stiffness on the Phenotype of Heart Cells. *Biotechnol. Bioeng.* **2010**, *105*, 1148–1160.
13. Rao, L.; Zhou, H.; Li, T.; Li, C.; Duan, Y. Y. Polyethylene Glycol-Containing Polyurethane Hydrogel Coatings for Improving the Biocompatibility of Neural Electrodes. *Acta Biomater.* **2012**, *8*, 2233–2242.
14. Bellamkonda, R. V.; Pai, S. B.; Renaud, P. Materials for Neural Interfaces. *MRS Bull.* **2012**, *37*, 557–561.
15. Poole-Warren, L.; Lovell, N.; Baek, S.; Green, R. Development of Bioactive Conducting Polymers for Neural Interfaces. *Expert Rev. Med. Devices* **2010**, *7*, 35–49.
16. Kotov, N. A.; Winter, J. O.; Clements, I. P.; Jan, E.; Timko, B. P.; Campidelli, S.; Pathak, S.; Mazzatenta, A.; Lieber, C. M.; Prato, M.; *et al.* Nanomaterials for Neural Interfaces. *Adv. Mater.* **2009**, *21*, 3970–4004.
17. Guiseppi-Elie, A. Electroconductive Hydrogels: Synthesis, Characterization and Biomedical Applications. *Biomaterials* **2010**, *31*, 2701–2716.
18. Seliktar, D. Designing Cell-Compatible Hydrogels for Biomedical Applications. *Science* **2012**, *336*, 1124–1128.
19. Mawad, D.; Stewart, E.; Officer, D. L.; Romeo, T.; Wagner, P.; Wagner, K.; Wallace, G. G. A Single Component Conducting Polymer Hydrogel as a Scaffold for Tissue Engineering. *Adv. Funct. Mater.* **2012**, *22*, 2692–2699.
20. Sekine, S.; Ido, Y.; Miyake, T.; Nagamine, K.; Nishizawa, M. Conducting Polymer Electrodes Printed on Hydrogel. *J. Am. Chem. Soc.* **2010**, *132*, 13174–13175.
21. Xu, Y.; Lin, Z.; Huang, X.; Liu, Y.; Huang, Y.; Duan, X. Flexible Solid-State Supercapacitors Based on Three-Dimensional Graphene Hydrogel Films. *ACS Nano* **2013**, *7*, 4042–4049.
22. Ghosh, S.; Rasmusson, J.; Inganäs, O. Supramolecular Self-Assembly for Enhanced Conductivity in Conjugated Polymer Blends: Ionic Crosslinking in Blends of Poly(3,4-ethylenedioxythiophene)-poly(styrenesulfonate) and Poly(vinylpyrrolidone). *Adv. Mater.* **1998**, *10*, 1097–1099.
23. Ghosh, S.; Inganäs, O. Conducting Polymer Hydrogels as 3D Electrodes: Applications for Supercapacitors. *Adv. Mater.* **1999**, *11*, 1214–1218.
24. Ghosh, S.; Inganas, O. Electrochemical Characterization of Poly(3,4-ethylene dioxythiophene) Based Conducting Hydrogel Networks. *J. Electrochem. Soc.* **2000**, *147*, 1872–1877.
25. Xia, Y.; Zhu, H. Polyaniline Nanofiber-Reinforced Conducting Hydrogel with Unique pH-Sensitivity. *Soft Matter* **2011**, *7*, 9388–9393.
26. Kishi, R.; Hiroki, K.; Tominaga, T.; Sano, K.-I.; Okuzaki, H.; Martinez, J. G.; Otero, T. F.; Osada, Y. Electro-Conductive Double-Network Hydrogels. *J. Polym. Sci., Polym. Phys.* **2012**, *50*, 790–796.
27. Naficy, S.; Razal, J. M.; Spinks, G. M.; Wallace, G. G.; Whitten, P. G. Electrically Conductive, Tough Hydrogels with pH Sensitivity. *Chem. Mater.* **2012**, *24*, 3425–3433.
28. Green, R. A.; Hassarati, R. T.; Goding, J. A.; Baek, S.; Lovell, N. H.; Martens, P. J.; Poole-Warren, L. A. Conductive Hydrogels: Mechanically Robust Hybrids for Use as Biomaterials. *Macromol. Biosci.* **2012**, *12*, 494–501.
29. Guo, B.; Finne-Wistrand, A.; Albertsson, A.-C. Facile Synthesis of Degradable and Electrically Conductive Polysaccharide Hydrogels. *Biomacromolecules* **2011**, *12*, 2601–2609.
30. Marcasuzaa, P.; Reynaud, S.; Ehrenfeld, F.; Khoukh, A.; Desbrieres, J. Chitosan-*graft*-Polyaniline-Based Hydrogels: Elaboration and Properties. *Biomacromolecules* **2010**, *11*, 1684–1691.
31. Pan, L.; Yu, G.; Zhai, D.; Lee, H. R.; Zhao, W.; Liu, N.; Wang, H.; Tee, B. C. K.; Shi, Y.; Cui, Y.; *et al.* Hierarchical Nanostructured Conducting Polymer Hydrogel with High Electrochemical Activity. *Proc. Natl. Acad. Sci. U.S.A.* **2012**, *109*, 9287–9292.
32. Siddhanta, S. K.; Gangopadhyay, R. Conducting Polymer Gel: Formation of a Novel Semi-IPN from Polyaniline and Crosslinked Poly(2-acrylamido-2-methyl propanesulphonicacid). *Polymer* **2005**, *46*, 2993–3000.
33. Mano, N.; Yoo, J. E.; Tarver, J.; Loo, Y.-L.; Heller, A. An Electron-Conducting Cross-Linked Polyaniline-Based Redox Hydrogel, Formed in One Step at pH 7.2, Wires Glucose Oxidase. *J. Am. Chem. Soc.* **2007**, *129*, 7006–7007.
34. Chen, S.-A.; Lee, H.-T. Structure and Properties of Poly(acrylic acid)-Doped Polyaniline. *Macromolecules* **1995**, *28*, 2858–2866.
35. Petrova, J.; Romanova, J.; Madjarova, G.; Ivanova, A.; Tadjer, A. Absorption Spectra of Model Single Chains of Conducting Polyaniline. *J. Phys. Chem. B* **2012**, *116*, 6543–6552.
36. Cao, Y.; Andreatta, A.; Heeger, A. J.; Smith, P. Influence of Chemical Polymerization Conditions on the Properties of Polyaniline. *Polymer* **1989**, *30*, 2305–2311.
37. Ding, H.; Wan, M.; Wei, Y. Controlling the Diameter of Polyaniline Nanofibers by Adjusting the Oxidant Redox Potential. *Adv. Mater.* **2007**, *19*, 465–469.
38. Ding, H.; Shen, J.; Wan, M.; Chen, Z. Formation Mechanism of Polyaniline Nanotubes by a Simplified Template-Free Method. *Macromol. Chem. Physic.* **2008**, *209*, 864–871.
39. Wang, Y. G.; Li, H. Q.; Xia, Y. Y. Ordered Whiskerlike Polyaniline Grown on the Surface of Mesoporous Carbon and Its Electrochemical Capacitance Performance. *Adv. Mater.* **2006**, *18*, 2619–2623.
40. Bhadra, S.; Khastgir, D.; Singha, N. K.; Lee, J. H. Progress in Preparation, Processing and Applications of Polyaniline. *Prog. Polym. Sci.* **2009**, *34*, 783–810.
41. Pan, L. J.; Pu, L.; Shi, Y.; Sun, T.; Zhang, R.; Zheng, Y. O. Hydrothermal Synthesis of Polyaniline Mesostructures. *Adv. Funct. Mater.* **2006**, *16*, 1279–1288.
42. Shi, W.; Ge, D.; Wang, J.; Jiang, Z.; Ren, L.; Zhang, Q. Heparin-Controlled Growth of Polypyrrole Nanowires. *Macromol. Rapid Commun.* **2006**, *27*, 926–930.
43. Canal, T.; Peppas, N. A. Correlation between Mesh Size and Equilibrium Degree of Swelling of Polymeric Networks. *J. Biomed. Mater. Res.* **1989**, *23*, 1183–1193.
44. Wang, D.-W.; *et al.* Fabrication of Graphene/Polyaniline Composite Paper *via in Situ* Anodic Electropolymerization for High-Performance Flexible Electrode. *ACS Nano* **2009**, *3*, 1745–1752.
45. Kim, D.-H.; Abidian, M.; Martin, D. C. Conducting Polymers Grown in Hydrogel Scaffolds Coated on Neural Prosthetic Devices. *J. Biomed. Mater. Res., Part A* **2004**, *71A*, 577–585.

46. Green, R. A.; Lovell, N. H.; Wallace, G. G.; Poole-Warren, L. A. Conducting Polymers for Neural Interfaces: Challenges in Developing an Effective Long-Term Implant. *Biomaterials* **2008**, *29*, 3393–3399.
47. Abidian, M. R.; Martin, D. C. Experimental and Theoretical Characterization of Implantable Neural Microelectrodes Modified with Conducting Polymer Nanotubes. *Biomaterials* **2008**, *29*, 1273–1283.
48. Rubinson, J. F.; Kayinamura, Y. P. Charge Transport in Conducting Polymers: Insights from Impedance Spectroscopy. *Chem. Soc. Rev.* **2009**, *38*, 3339–3347.
49. Rammelt, U.; Reinhard, G. On the Applicability of a Constant Phase Element (CPE) to the Estimation of Roughness of Solid Metal Electrodes. *Electrochim. Acta* **1990**, *35*, 1045–1049.
50. Bisquert, J.; Garcia-Belmonte, G.; Bueno, P.; Longo, E.; Bulhaues, L. O. S. Impedance of Constant Phase Element (CPE)-Blocked Diffusion in Film Electrodes. *J. Electrochem. Soc.* **1998**, *452*, 229–234.
51. Albery, W. J.; Chen, Z.; Horrocks, B. R.; Mount, A. R.; Wilson, P. J.; Bloor, D.; Monkman, A. T.; Elliott, C. M. Spectroscopic and Electrochemical Studies of Charge Transfer in Modified Electrodes. *Faraday Discuss.* **1989**, *88*, 247–259.
52. Paasch, G.; Micka, K.; Gersdorf, P. Theory of the Electrochemical Impedance of Macrohomogeneous Porous Electrodes. *Electrochim. Acta* **1993**, *38*, 2653–2662.
53. Friedrich, B. M.; Safran, S. A. How Cells Feel Their Substrate: Spontaneous Symmetry Breaking of Active Surface Stresses. *Soft Matter* **2012**, *8*, 3223–3230.
54. Park, M.-K.; Onishi, K.; Locklin, J.; Caruso, F.; Advincula, R. C. Self-Assembly and Characterization of Polyaniline and Sulfonated Polystyrene Multilayer-Coated Colloidal Particles and Hollow Shells. *Langmuir* **2003**, *19*, 8550–8554.
55. Wei, Z.; Wan, M.; Lin, T.; Dai, L. Polyaniline Nanotubes Doped with Sulfonated Carbon Nanotubes Made *via* a Self-Assembly Process. *Adv. Mater.* **2003**, *15*, 136–139.
56. Long, Y.; Zhang, L.; Ma, Y.; Chen, Z.; Wang, N.; Zhang, Z.; Wan, M. Electrical Conductivity of an Individual Polyaniline Nanotube Synthesized by a Self-Assembly Method. *Macromol. Rapid Commun.* **2003**, *24*, 938–942.
57. McCullough, L. A.; Dufour, B.; Matyjaszewski, K. Polyaniline and Polypyrrole Templated on Self-Assembled Acidic Block Copolymers. *Macromolecules* **2009**, *42*, 8129–8137.
58. McCullough, L. A.; Matyjaszewski, K. Conjugated Conducting Polymers as Components in Block Copolymer Systems. *Mol. Cryst. Liq. Cryst.* **2010**, *521*, 1–55.
59. McCullough, L. A.; Dufour, B.; Tang, C.; Zhang, R.; Kowalewski, T.; Matyjaszewski, K. Templating Conducting Polymers *via* Self-Assembly of Block Copolymers and Supramolecular Recognition. *Macromolecules* **2007**, *40*, 7745–7747.
60. Yoo, J. E.; Cross, J. L.; Bucholz, T. L.; Lee, K. S.; Espe, M. P.; Loo, Y.-L. Improving the Electrical Conductivity of Polymer Acid-Doped Polyaniline by Controlling the Template Molecular Weight. *J. Mater. Chem.* **2007**, *17*, 1268–1275.
61. Kim, M.; Kim, Y.-J.; Gwon, K.; Tae, G. Modulation of Cell Adhesion of Heparin-Based Hydrogel by Efficient Physisorption of Adhesive Proteins. *Macromol. Res.* **2012**, *20*, 271–276.
62. Li, M.; Guo, Y.; Wei, Y.; MacDiarmid, A. G.; Lelkes, P. I. Electrospinning Polyaniline-Contained Gelatin Nanofibers for Tissue Engineering Applications. *Biomaterials* **2006**, *27*, 2705–2715.
63. Kim, D.-H.; Wiler, J. A.; Anderson, D. J.; Kipke, D. R.; Martin, D. C. Conducting Polymers on Hydrogel-Coated Neural Electrode Provide Sensitive Neural Recordings in Auditory Cortex. *Acta Biomater.* **2010**, *6*, 57–62.
64. Bettinger, C. J.; Bao, Z. Organic Thin-Film Transistors Fabricated on Resorbable Biomaterial Substrates. *Adv. Mater.* **2010**, *22*, 651–655.
65. Guo, B.; Glavas, L.; Albertsson, A.-C. Biodegradable and Electrically Conducting Polymers for Biomedical Applications. *Prog. Polym. Sci.* **2013**, *38*, 1263–1286.
66. Kim, Y. J.; Chun, S.-E.; Whitacre, J.; Bettinger, C. J. Self-Deployable Current Sources Fabricated from Edible Materials. *J. Mater. Chem. B* **2013**, *1*, 3781–3788.
67. Kim, Y. J.; Wu, W.; Chun, S.-E.; Whitacre, J. F.; Bettinger, C. J. Biologically-Derived Melanin Electrodes in Aqueous Sodium-Ion Energy Storage Devices. *Proc. Natl. Acad. Sci. U.S.A.* **2013**, *110*, 20912–20917.
68. Famm, K.; Litt, B.; Tracey, K. J.; Boyden, E. S.; Slaoui, M. Drug Discovery: A Jump-Start for Electroceuticals. *Nature* **2013**, *496*, 159–161.
69. Wu, H.; Yu, G.; Pan, L.; Liu, N.; McDowell, M. T.; Bao, Z.; Cui, Y. Stable Li-Ion Battery Anodes by *in Situ* Polymerization of Conducting Hydrogel To Conformally Coat Silicon Nanoparticles. *Nat. Commun.* **2013**, *4*, 1943.